Breaking the Far-Field Diffraction Limit in Optical Nanopatterning via Repeated Photochemical and Electrochemical Transitions in Photochromic Molecules

Nicole Brimhall, Trisha L. Andrew, Rajakumar Varma Manthena, and Rajesh Menon

Phys. Rev. Lett. **107**, 205501 — Published 7 November 2011

DOI: 10.1103/PhysRevLett.107.205501

Breaking the far-field diffraction limit in optical nanopatterning via repeated photochemical and electrochemical transitions in photochromic molecules

Nicole Brimhall[1], Trisha L. Andrew[2], Rajakumar Varma Manthena[1], and Rajesh Menon[1]

[1]Department of Electrical and Computer Engineering, University of Utah, Salt Lake City, UT 84112, USA. [2]Department of Chemistry, Massachusetts Institute of Technology, Cambridge, MA 02139, USA.

Abstract: By saturating a photochromic transition with a nodal illumination (wavelength, λ), one isomeric form of a small molecule is spatially localized to a region smaller than the far-field diffraction limit. A selective oxidation step effectively "locks" this pattern allowing repeated patterning. Using this approach and a two-beam interferometer, we demonstrate isolated lines as narrow as λ/8 (78nm) and spacing between features as narrow as λ/4 (153nm). This is considerably smaller than the minimum far-field diffraction limit of λ/2. Most significantly, nanopatterning is achieved via single-photon reactions and at low light levels, which in turn, allow for high throughput.

PACS numbers: 42.50.St, 81.16.Nd, 42.70.Jk

Deterministic manipulation of matter at the nanoscale over macroscopic areas can lead to new material properties, enabling unique functionalities. However, patterning nanostructures over macroscopic areas remains challenging. As opposed to pattern-replication, pattern-generation is, in general, slow. Scanning-electron-beam lithography (SEBL), which is the dominant method for pattern-generation at the nanoscale, is a serial slow process. Also, electrons are readily deflected by extraneous electromagnetic fields, limiting the accuracy with which patterns can be placed relative to one another [1,2]. Patterning with photons, on the other hand, can be fast due to the availability of lasers and the potential for massive parallelism [3]. However, diffraction precludes light from

patterning features smaller than $\lambda/(2NA)$, the so-called Abbé or far-field diffraction limit when using conventional imaging techniques [4]. Here, NA is the numerical aperture of the imaging system.

The far-field diffraction barrier can be overcome in the near-field [5]. However, the small distances involved make such approaches challenging to parallelize, which is essential for high speed. Two-photon lithography can also overcome this limit, but at the cost of very high light intensities [6]. Recently, two alternate methods that have the potential to overcome the diffraction limit in the far-field have been proposed. These methods both rely on the exposure of a node, which was first demonstrated in atom lithography [7-10]. The first method exploits the photo-induced activation and deactivation of polymerization reactions [11-14]. Photopolymerization induced within the focal volume of a first beam is deactivated except near the center by a second aligned nodal illumination. The overall effect is to limit polymerization to a region that is smaller than the width of the diffraction-limited focal spot. The nodal beam must have high intensity to efficiently deactivate the polymerization reaction before it proceeds to completion. Therefore, this approach is difficult to parallelize. Furthermore, the poor spectral selectivity of the activation and deactivation reactions leads to low image contrast, which has so far limited this approach to patterning isolated features.

The second method, absorbance modulation [15-18], employs a layer of photochromic molecules that are placed atop a separate photoresist film. As indicated in Fig. 1(A), these molecules can be switched between two isomeric forms by illumination at two wavelengths. When the photochromic film is simultaneously exposed to a spot at one wavelength (λ_1) and a node at another wavelength (λ_2), it is possible to spatially

localize one of the isomers within a narrow region in the vicinity of the node. Since this isomer is more transparent to λ_1 compared to the other, the transmitted light at λ_1 is localized to the same narrow region, and can be recorded in the underlying photoresist. This approach is currently limited by the low quantum efficiency of one of the two photo-reactions. This, in turn, necessitates high-intensity in the nodal beam.

Microscopy beyond the far-field diffraction limit has been enabled by saturating an optical transition such as fluorescence [19]. It was also proposed that if this saturated transition was coupled with a "locking" step, optical nanopatterning would be possible [20]. Here, we report an implementation of this idea, which we call Patterning via Optical Saturable Transitions (POST). In the current implementation of POST, the recording medium is a photochromic film composed of 1,2-bis(5,5′-dimethyl-2,2'-bithiophen-yl) perfluorocyclopent-1-ene (compound **1**) shown in Fig. 1(A) [21].

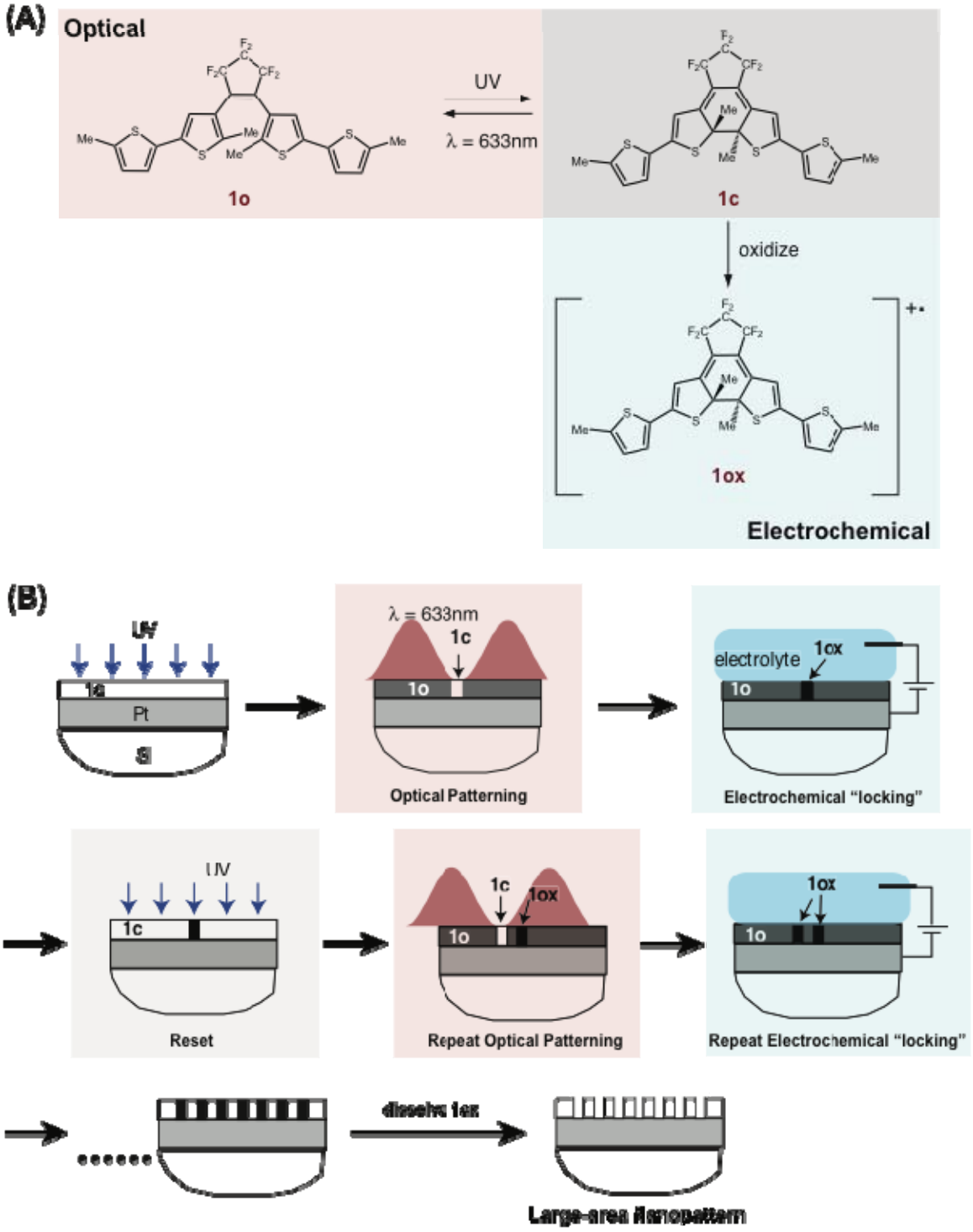

Figure 1:

Compound **1** exists in two isomeric forms, open-ring (**1o**) and closed-ring (**1c**). Due to the extended conjugation of **1c**, it can be selectively oxidized to a stable cation

(**1ox**) as indicated in Fig. 1(A) [22]. The sequence of steps involved in POST is illustrated in Fig. 1(B). The sample is typically a silicon wafer coated with a thin platinum film and a photochromic overlayer [21]. First, the molecules are converted to **1c** by uniform illumination with a short-wavelength UV lamp (UVP UVGL-25). Then, the sample is exposed to a nodal illumination at $\lambda = 633$ nm (Melles-Griot 05-LHP-151). This converts all the molecules to **1o** except in the vicinity of the node, where they remain in **1c**. In other words, by saturating the photochemical transition from **1c** to **1o**, we can confine the molecules in **1o** to a sub-wavelength region at the node. A subsequent electrochemical oxidation step converts only those molecules remaining in form **1c** into the stable radical cation, **1ox**. Note that **1ox** is not photochromic, and therefore does not participate in any further photo-reactions. The three steps are repeated with intervening displacements of the sample, as illustrated. This leads to regions of **1ox** interspersed within the layer of **1o**. After all the exposures are completed, the regions of **1ox** are selectively dissolved away in a polar solvent. The remaining film could serve as a resist to a subsequent pattern-transfer step [23, 24]. With POST, the spacing between the features is limited primarily by the quality of the node and not by diffraction. Furthermore, the two isomers are thermally stable and only single-photon reactions are involved. This allows for high resolution at low light intensities.

The simulated distribution of the relative concentration of **1ox** after a single exposure/oxidation cycle is shown in Fig. 2(a) [21]. Material properties of compound **1** as well as an incident standing wave at $\lambda = 633$ nm with a period of 600 nm were assumed. **1ox** is primarily localized to a small region at the node of the illumination. The distribution shows a unique undercut profile, which was experimentally verified as

described later. In POST, the "node" is recorded to create the feature. Hence, the feature size decreases with increasing exposure dose. This is simulated in Fig. 2(b), where the full-width at half-maximum (FWHM) of the distribution of **1ox** at the top of the layer is plotted as a function of the relative exposure dose. Note that the FWHM decreases beyond the far-field diffraction limit of the simulated system, *i.e.*, 300nm. In fact, the smallest achievable width is limited primarily by the quality of the node. Figures 2(c)-(d) show that the linewidths decrease as the exposure dose is increased. Lines as small as 78nm were also resolved as shown in Fig. 2(f). Further details of the experiments are given below.

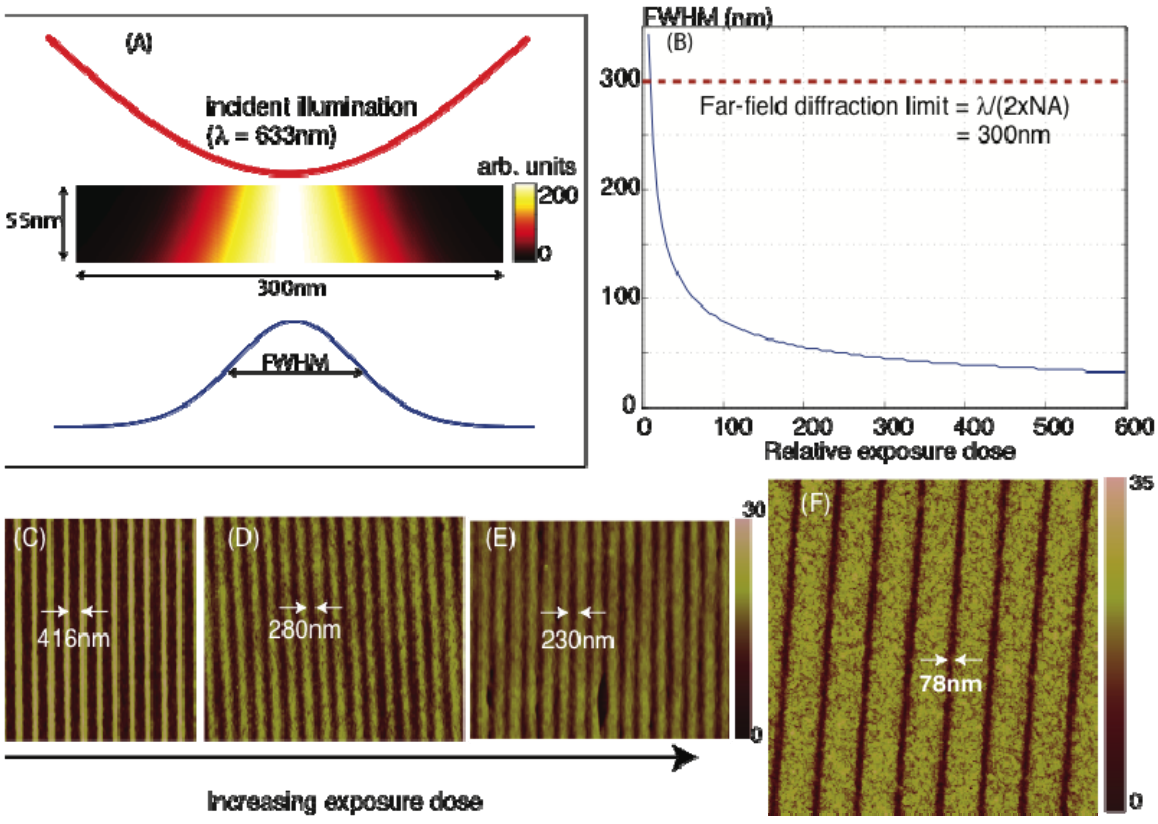

Figure 2:

Cyclic voltammograms (CVs) of both isomers in dichloromethane (DCM), shown in Fig. 3(a), confirmed that the first oxidation peak of the closed form occurs at 0.97V

(vs. Ag/AgCl), which is 0.3V lower than the first oxidation peak of the open form [21]. At 0.97V the closed form is preferentially oxidized into a stable radical cation [25]. Thin films of **1c** deposited on platinum or ITO electrodes were oxidized by immersing in purified water with platinum or ITO as the working electrode, a platinum wire counter electrode, and a Ag/AgCl reference electrode [21]. Thin films of **1c**, **1o**, and **1ox** were further characterized via ultraviolet-visible (UV-Vis) absorption spectroscopy (Fig. 3(b)). The spectra confirm the existence of three distinct and stable states (also evident by their distinct colors in the optical micrographs).

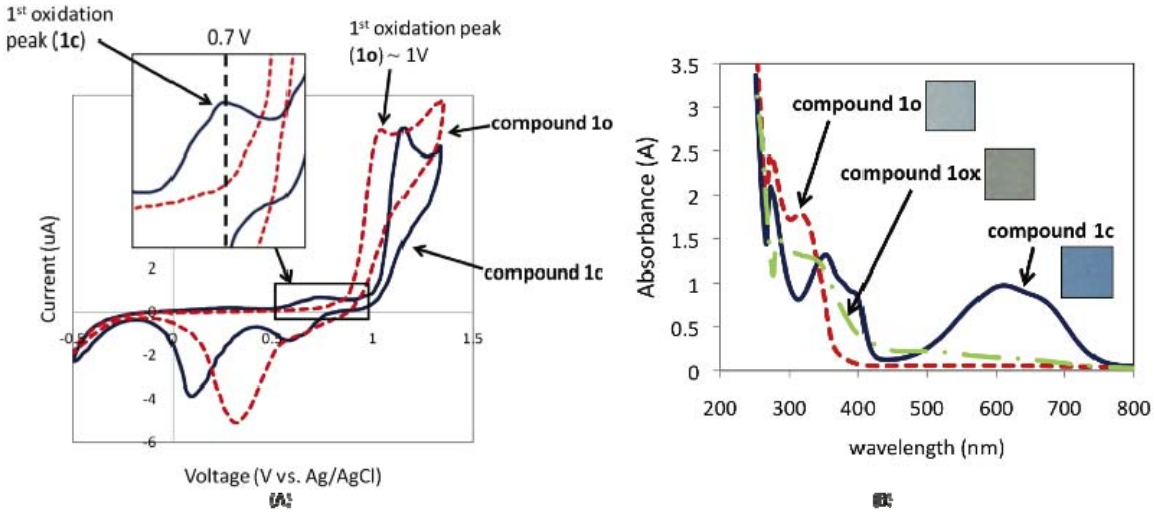

Figure 3:

For patterning experiments, we thermally evaporated 45 to 55nm thick layers of of compound **1** at 73°C onto a substrate composed of 100nm of platinum on a silicon wafer. Then, samples were irradiated with short-wavelength UV light for about 5 mins to fully convert the film to **1c**. A Lloyd's-mirror interferometer with a helium-neon laser was used to generate a standing wave with a period of ~610 nm [21]. After exposure, the sample was electrochemically oxidized at V_{ox} for ten minutes in an electrolyte with the platinum layer as the working electrode, a platinum wire counter electrode, and a

Ag/AgCl reference electrode. The peak oxidation voltage, V_{ox}, was determined by performing cyclic voltammetry on a test sample from each evaporation batch, and it varied between 0.9V and 1.1V. The electrolyte was either purified water or a dilute NaCl solution. Finally, the sample was developed in a mixture of 5% isopropyl alcohol and 95% ethylene glycol by volume for 60 seconds.

The lines in figures 2(C)-(E) were exposed with an incident power density of 4.5mW/cm^2 and exposure times of 30mins, 45mins and 50mins, respectively. The samples were oxidized at 0.93V for 10 mins and finally, developed as usual. Isolated lines with widths as narrow as 78 nm (or $\lambda/8$) were clearly resolved with a single exposure as illustrated in the atomic-force micrograph in Fig. 2(F). In this case, the exposure time was 315s at an incident intensity of ~45mW/cm^2. This particular sample was oxidized at V_{ox} = 1.08V for 10 minutes in a 0.04M NaCl solution. Fig. 4(a) shows a two-step exposure where the sample was rotated by about 25 degrees between the exposures. The exposure time for each step was 45 mins at an incident intensity of 4.5mW/cm^2. The sample was exposed to the short-UV lamp for 6 mins after the first exposure and oxidation. The oxidation conditions were V_{ox} = 0.91V for 5 mins in purified water. Finally, the sample was developed as usual. As indicated in the top schematic, this dual-exposure process should result in a crossed-line pattern, where the spacing between adjacent lines decrease to zero. The corresponding atomic-force micrograph in Fig. 4(B) resolves lines with spacing as small as 153nm or $\lambda/4$, about half the far-field diffraction limit. On a separate sample, we performed two consequent exposures (exposure time = 67 minutes each, incident intensity = 4.5mW/cm^2) with intervening oxidation steps (V_{ox}=1.1V for 10 minutes each in purified water). The sample

was exposed to the UV lamp for 6 minutes before the second exposure. In this case, the sample was removed from the exposure system for the oxidation step. When it was placed back in the exposure system for the second exposure, random displacements were introduced. After the final dissolution step, the sample was examined thoroughly, and a portion is shown in the atomic-force micrograph in Fig. 4(b). The spacing between the lines is 263nm, which is less than half the far-field diffraction limit of $\lambda/(2NA) = 610$nm. Fig. 4(c) shows a scanning-electron micrograph of the cross-section of a single-exposure line of width 89nm. This sample was exposed for 65 minutes at an incident power of 4.5mW/cm^2, and oxidized at V_{ox}=0.93V for 10 minutes in purified water. The undercut feature, which was predicted by the simulations in Fig. 2(a) is confirmed as shown in Fig. 4(D). This feature could be advantageous for pattern transfer using lift-off. The patterned area in all these samples were limited by the width of the incident beam, and uniform lines were observed over areas as large as 0.5mm^2 (corresponding approximately to a semi-circle of radius 0.6mm).

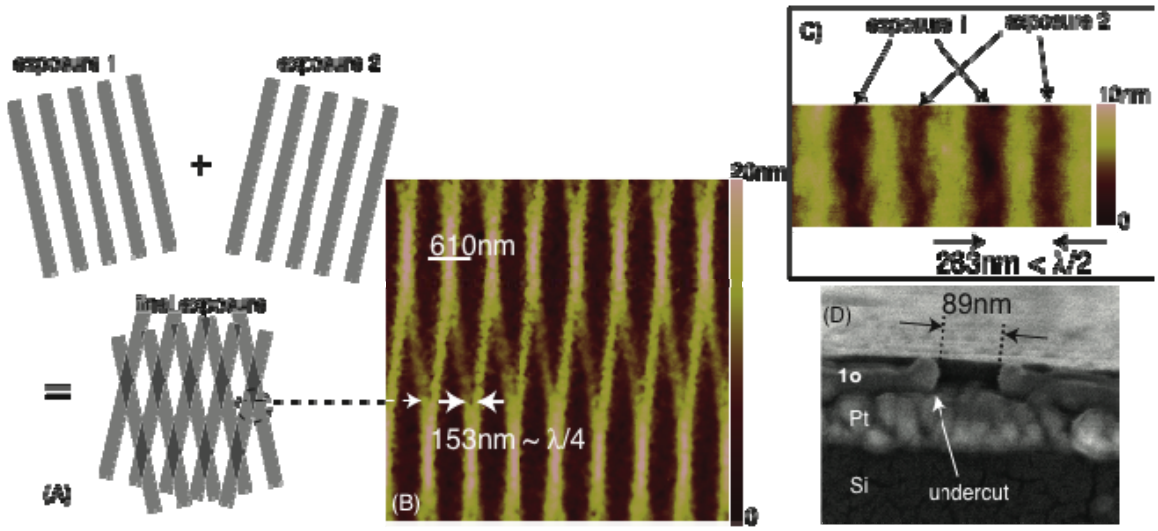

Figure 4:

It must be noted that in the semiconductor industry, lithography is currently performed with ~70nm spacing between features [26]. This is achieved using a diffraction-limited image-replication process that utilizes 193nm illumination wavelength under water immersion. The original pattern is typically created via scanning-electron-beam lithography, which is too slow for manufacturing. In order to replicate patterns at even smaller feature-spacings, shorter wavelengths are necessary, which give rise to enormous challenges in implementation [27]. Alternative proposals rely on massively parallel electron beams with their concomitant disadvantages [28]. POST offers an elegant alternative with the promise of relatively fast, large-area diffraction-unlimited nanopatterning with low-cost UV lamps and visible-light sources.

In conclusion, we demonstrated optical patterning of isolated lines as small as $\lambda/8$ and adjacent features spaced by as small as $\lambda/4$ with single-photon transitions (low light intensities) and simple electrochemistry. Improved illumination conditions and materials optimization should enable scaling of features far below 100nm. Our approach opens the door to high-speed large-area nanopatterning via parallelism. An array of independently controllable nodes can enable parallel patterning of complex geometries in a "dot-matrix" fashion [29]. Although the current demonstration utilized one-dimensional standing waves, we anticipate straightforward extension to two- and three- dimensional patterning using either diffractive optics [30-32] or phase-masks [33].

Acknowledgements. We thank Deborah Mascaro for use of the low-temperature evaporator, Jennifer Schumaker-Perry for use of the UV-Vis spectrometer, Mohit Diwekar for assistance with platinum sputtering, Brian Van Devener for assistance with

atomic-force microscopy, Randy Polson for assistance with scanning-electron microscopy, and Brian Baker, Paul Cole, and Charles Fisher for help in the Utah microfabrication facility. N. B. and R. V. M. were supported by the Utah Science Technology and Research (USTAR) initiative. R.V.M was partially supported by a DARPA contract No. N66001-10-1-4065.

References:

[1] K. Murooka, K. Hattori, and O. Iizuka, J. Vac. Sci. Technol. B. **21,** 2668 (2003).

[2] J. T. Hastings, F. Zhang, and H. I. Smith, J. Vac. Sci. Technol. B. **21**, 2650–2656 (2003).

[3] H. I. Smith, R. Menon, A. Patel, D. Chao, M. Walsh, and G. Barbastathis, Microelectron. Eng. **83,** 956-961 (2006).

[4] E. Abbé, Beiträge zur Theorie des Mikroskops und der mikroskopischen Wahrnehmung. *Arch. mikrosk. Anat. Entwichlungsmech.* **9,** 413-468 (1873).

[5] E. A. Ash, and G. Nichols, Nature **237**, 510 (1972).

[6] S. Kawata, H. B. Sun, T. Tanaka, and T. Takada, Nature **412**, 697 (2001).

[7] K. K. Berggren, A. Bard, J. L. Wilbur, J. D. Gillaspy, A. G. Helg, J. J. McClelland, S. L. Rolston, W. D. Phillips, M. Prentiss, and G. M. Whitesides, Science **269**, 1255 (1995).

[8] U. Drodofsky, J. Stuhler, B. Brezger, Th. Schulze, M. Drewsen, T. Pfau and J. Mlynek, *Microelectron. Eng.* **35**, 285 (1997).

[9] Th. Schulze, B. Brezger, R. Mertens, M. Pivk, T. Pfau and J. Mlynek, *Appl. Phys. B* **70**, 671 (2000).

[10] M. K. Oberthaler and T. Pfau, *J. Phys. Condens. Matter*, **15**, R233 (2003).

[11] J. T. Fourkas, J. Phys. Chem. Lett. **1**, 1221 (2010).

[12] L. J. Li, R. R. Gattass, E. Gershgoren, H. Hwang, and J. T. Fourkas, *Science* **324**, 910–913 (2009).

[13] T. F. Scott, B. A. Kowalski, A. C. Sullivan, C. N. Bowman, and R. R. McLeod, Science **324**, 913–917 (2009).

[14] J. Fischer, G. von Freymann, and M. Wegener, Adv. Mater. **22**, 3578-3582 (2010).

[15] T. L. Andrew, H-Y. Tsai, and R. Menon, Science **324**, 917 (2009).

[16] R. Menon, and H. I. Smith, J. Opt. Soc. Am. A. **23**, 2290-2294 (2006).

[17] R. Menon, H-Y. Tsai, and S. W. Thomas III, Phys. Rev. Lett. **98**, 043905 (2007).

[18] H-Y. Tsai, G. W. Walraff, and R. Menon, Appl. Phys. Lett., **91**, 094103 (2007).

[19] S. W. Hell, Science **316**, 1153 (2007).

[20] S. W. Hell, Phys. Lett. A **326** (1-2), 140 (2004).

[21] See Supplemental Material at [URL will be inserted by publisher] for further information.

[22] T. Saika, M. Irie, and T. Shimidzu, J. Chem. Commun. **1994**, 2123-2124 (1994).

[23] T. Ito, T. Yamada, Y. Inao, T. Yamaguchi, N. Mizutani, and R. Kuroda, Appl. Phys. Lett. **89**, 033113 (2006).

[24] D. Pires, J. L. Hedrick, A. De Silva, J. Frommer, B. Gotsmann, H. Wolf, M. Despont, U. Duerig, and A. W. Knoll, Science **328**, 732 (2010).

[25] W. R. Browne, J. J. D. de Jong, T. Kudernac, M. Walko, L. N. Lucas, K. Uchida, J. H. van Esch, B. L. Feringa, Chem. Eur. J. **11**, 6430 – 6441 (2005).

[26] International Technology Roadmap for Semiconductors. http://public.itrs.net/

[27] E. S. Putna, T. R. Younkin, M. Leeson, R. Caudillo, T. Bacuita, U. Shah, and M. Chandhok, Proc. SPIE **7969,** 79692K (2011).

[28] R. Freed, J. Sun, A. Brodie, P. Petric, M. McCord, K. Ronse, L. Haspeslagh, B. Vereecke, Proc. SPIE **7970**, 79701T (2011).

[29] R. Menon, A. A. Patel, D. Gil, and H. I. Smith, Materials Today 8, 26 (2005).

[30] H-Y. Tsai, H.I. Smith, and R. Menon, J. Vac. Sci. Technol. B **25**, 2068 (2007).

[31] H-Y. Tsai, H. I. Smith, and R. Menon, Opt. Lett. **33**, 2916 (2008).

[32] H-Y. Tsai, S. W. Thomas III, and R. Menon, Opt. Exp. **18,** 16015 (2010).

[33] S. W. Hell, R. Schmidt, and A. Egner, Nature Photonics **3**, 381 (2009).

Supplementary Information accompanies the paper online.

Competing Interests statement. None.

Author Contributions. N. B. designed and performed experiments, analyzed results and wrote the manuscript. T. L. A. synthesized and characterized the photochromic molecules and edited the manuscript. R. V. M. performed sample preparation. R. M. designed experiments, analyzed results, performed simulations, and wrote the manuscript.

Correspondence and requests for materials should be addressed to R. M. (rmenon@eng.utah.edu).

Figure Legends:

FIG. 1. (Color online) Patterning via optical-saturable transitions (POST). (a) Scheme of the photochromic molecule, compound **1**. (b) Sequence of steps for POST. Uniform UV illumination converts all molecules to **1c**. A node at λ = 633 nm converts all molecules to **1o** except at the node. Electrochemical oxidation

selectively converts **1c** to **1ox**. These three steps are repeated with intervening displacements of the sample to create dense features whose spacing is smaller than the diffraction limit. A polar solvent selectively dissolves **1ox** resulting in nanoscale topography.

FIG. 2. (Color online) Simulation and electrochemical characterization of POST. (a) Simulated distribution of **1ox** at the end of a single exposure-oxidation cycle. The incident illumination is a standing wave of period 600nm (λ = 633nm). The cross-section of the **1ox** distribution at the top of the film is shown below. (b) FWHM as a function of relative exposure dose with the same illumination conditions as in (a). (c)-(e) Atomic-force micrographs of isolated lines patterned using POST. Note that the linewidths decrease with increasing exposure dose. (f) Atomic-force micrograph of isolated lines of width 78nm. Experimental details are provided in the text.

FIG. 3. (Color online) Characterization of the three isomeric forms of compound **1**. (a) Cyclic voltammograms of both open- and closed-isomers in solution (0.3mM compound **1** in 0.1 M $TBAPF_6$ in DCM, platinum button working electrode, 100mV/sec). The closed form is oxidized at 0.97V while the open form is oxidized at 1.28V. (b) UV-Vis absorbance curves of 80nm of compound **1** thermally evaporated onto an ITO-coated glass slide show clear distinctions between the three forms. Optical micrographs of the three forms (insets) also show distinct colorations.

FIG. 4. Experimental confirmation of sub-diffraction-limited optical nanopatterning. (a) Two-step exposure process where the sample is rotated in between the exposures. An intervening oxidation step “fixes” the first exposed

pattern such that it is minimally perturbed by the next exposure. A 6-min UV exposure is used to bring all the molecules back to the open state before the second exposure. (b) Atomic-force micrograph of the final pattern agrees well with the expected pattern. The smallest resolved spacing between features is about 153nm. (c) Atomic-force micrograph of a sample that underwent two exposures. The spacing between the lines is 263 nm, which is less than half the far-field diffraction limit in this case (610nm). (d) Cross-section scanning-electron micrograph of a single exposure line of width 89nm. The undercut predicted by the simulation in Fig. 2(a) is clearly observed. The experimental details are described in the text.